Journal of Biomechanics 162 (2024) 111882

Contents lists available at ScienceDirect

Journal of Biomechanics

journal homepage: www.elsevier.com/locate/jbiomech

Microscale strain concentrations in tissue-engineered osteochondral implants are dictated by local compositional thresholds and architecture

Byumsu Kim[a], Terri-Ann N. Kelly[b], Hyung Jin Jung[b], Olivia S. Beane[b], Sarindr Bhumiratana[b], Nikolaos Bouklas[a], Itai Cohen[c], Lawrence J. Bonassar[a,d,*]

[a] Sibley School of Mechanical and Aerospace Engineering, Cornell University, Ithaca, NY, United States
[b] EpiBone, Brooklyn, NY, United States
[c] Department of Physics, Cornell University, Ithaca, NY, United States
[d] Meinig School of Biomedical Engineering, Cornell University, Ithaca, NY, United States

ARTICLE INFO

Keywords:
Osteochondral Grafts
Tissue Engineering
FTIR
Digital Image Correlation
Cartilage Micromechanics
Biofabrication

ABSTRACT

Tissue-engineered osteochondral implants manufactured from condensed mesenchymal stem cell bodies have shown promise for treating focal cartilage defects. Notably, such manufacturing techniques have shown to successfully recapture the bulk mechanical properties of native cartilage. However, the relationships among architectural features, local composition, and micromechanical environment within tissue-engineered cartilage from cell-based aggregates remain unclear. Understanding such relationships is crucial for identifying critical parameters that can predict in vivo performance. Therefore, this study investigated the relationship among architectural features, composition, and micromechanical behavior of tissue-engineered osteochondral implants. We utilized fast-confocal microscopy combined with a strain mapping technique to analyze the micromechanical behavior under quasi-static loading, as well as Fourier Transform Infrared Spectroscopy to analyze the local compositions. More specifically, we investigated the architectural features and compositional distributions generated from tissue maturation along with macro- and micro-level strain distributions. Our results showed that under compression, cell-based aggregates underwent deformation followed by body movement, generating high local strain around the boundaries where local aggrecan concentration was low and local collagen concentration was high. By analyzing the micromechanics and composition at the single aggregate length scale, we identified a strong threshold relationship between local strain and composition, namely at the aggrecan concentration below 0.015 arbitrary unit (A.U.) and the collagen concentration above 0.15 A.U., constructs experienced greater than three-fold increase in compressive strain. Overall, this study suggests that local compositional features are the primary driver of the local mechanical environment in tissue-engineered cartilage constructs, providing insight into potential quality control parameters for manufacturing tissue-engineered constructs.

1. Introduction

For the last three decades, various tissue engineering approaches have been investigated to heal local cartilage defects. Scientists and engineers have utilized numerous biomaterials, ranging from hydrogels to synthetic scaffolds (Chu et al., 1995; Crawford et al., 2009; Jutila et al., 2015), as well as biofabrication methods, ranging from injection molding to 3D printing (Chang et al., 2003; Guo et al., 2017; Yan et al., 2023) to manufacture tissue-engineered cartilage. Multiple in vitro and in vivo studies have shown that functionally competent tissue-engineered constructs can be manufactured regardless of specific biofabrication methods (Kock et al., 2012; Little et al., 2011; Patel et al., 2019). Despite the tremendous success in cartilage biofabrication, identifying critical parameters that are predictive of product performance in vivo remains a major hurdle for the field (see Fig. 1). Notably, the Food and Drug Administration guidance in the past three decades suggests that the mechanical properties of the engineered cartilage tissue should be measured prior to implantation as they could

* Corresponding author at: Meinig School of Biomedical Engineering, Sibley School of Mechanical and Aerospace Engineering, 149 Weill Hall, Cornell University, Ithaca, NY 14853, United States.
E-mail address: lb244@cornell.edu (L.J. Bonassar).

https://doi.org/10.1016/j.jbiomech.2023.111882
Accepted 20 November 2023
Available online 24 November 2023

affect the success of the implantation (Center for Biologics Evaluation, 2019). Interestingly, multiple studies have shown that the macro level mechanical properties are strongly correlated to the overall composition of the engineered tissues, suggesting composition as a potential non-destructive parameter to predict mechanical properties (Kim and Bonassar, 2023; Rotter et al., 2002; Vunjak-Novakovic et al., 1999). However, to date, no tissue-engineered cartilage constructs have been able to replicate all mechanical properties of native tissue at multiple scales (Griffin et al., 2015; Little et al., 2011; Patel et al., 2019).

One of the challenges of replicating the mechanical properties of native cartilage tissue arises from the fact that the architectural and compositional distribution of tissue-engineered cartilage constructs do not match native tissue. Regardless of the biomaterials or fabrication methods, tissue-engineered cartilage constructs have extremely different architectural and compositional features compared to native tissue. Notably, clinically available tissue-engineered cartilage products or products that are in clinical trials all utilize collagen scaffolds (Crawford et al., 2012; Kon et al., 2012; Nurmukhametov et al., 2021). Previous studies have shown that collagen scaffold architecture creates compressive instabilities that are not observed in native tissue (Kim et al., 2023, 2022). More importantly, such local compositional thresholds are shown to have a strong correlation to the probability of instabilities for the tissue-engineered cartilage constructs (Middendorf et al., 2017). In addition, studies have shown that this local mechanical strain is predictive of cell death in native and tissue-engineered cartilage constructs (Bartell et al., 2015; Kim et al., 2023). These studies collectively indicate that identifying and monitoring the local compositional parameters are crucial for determining the quality of tissue-engineered cartilage.

Recent advances in a variety of scaffold-free technologies, such as pellet and micromass culture systems, have demonstrated to be a potential biofabrication approach for producing tissue-engineered cartilage constructs (Johnstone et al., 2013; Kim et al., 2011; Mohan-Raj et al., 2014). Notably, osteochondral tissue engineering technology, manufactured by using condensed mesenchymal stem cell bodies (CMBs) to trabecular bone scaffolds, have demonstrated promising in vivo results in the treatment of focal cartilage defects (Bhumiratana et al., 2014; Stefani et al., 2020). The grafts were then cultured for an extended period for stem cells differentiation and chondrogenic maturation. During the culture, CMBs integrate with each other and generate unique architectural features as well as cartilage matrix containing collagen and aggrecan. Remarkably, engineered cartilage tissue from CMBs have comparable bulk mechanical properties to that of native cartilage (Bhumiratana and Vunjak-Novakovic, 2015). Notably, the architecture of tissue grown from combining CMBs is distinct from native and tissue-engineered cartilage with collagen scaffolds. Investigating the relationships among the architectural features, local composition, and the micromechanical environment within tissue-engineered cartilage from CMBs is critical for identifying critical parameters that are predictive of in vivo performance.

As such, the objective of this study was to investigate the relationship among the architecture, local composition, and local micromechanical environment in tissue-engineered osteochondral grafts under unconfined compression testing. We obtained osteochondral grafts manufactured by using CMBs with trabecular bone scaffolds and investigated the relationship among architectural features, local composition, and local mechanical behavior. We (i) compared the architectural and compositional differences between the two different culture techniques, (ii) identified the global and local strain distribution, and (iii) found the correlation between the local composition and micromechanical behavior.

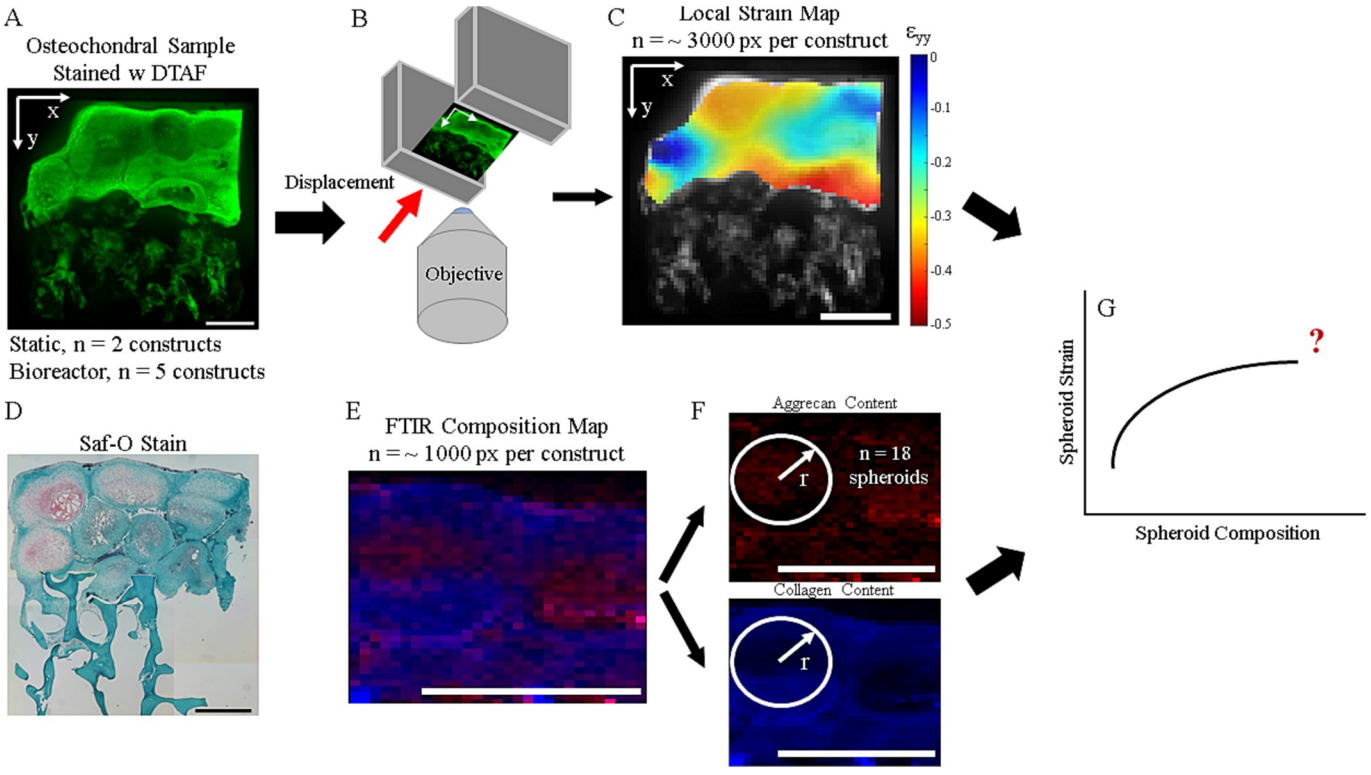

Fig. 1. Experimental and analysis methods for tissue-engineered osteochondral implants. A. Engineered osteochondral samples are manufactured using static and perfusion & loading culture conditions. B. Constructs were loaded in Tissue Deformation Imaging Stage and axially compressed. Compressive mechanical behavior of the samples was recorded. C. From the compression video, local strain was analyzed. D. Saf-O stain reveals heterogenous compositional distribution of osteochondral implant. E. The compositional distribution was quantified using Fourier Transform Infrared Spectroscopy. FTIR distribution data was linearly decomposed to aggrecan and collagen concentration and analyzed radially per spheroid basis. G. The relationship between radial composition and radial strain was found.

2. Materials and methods

2.1. Tissue-engineered osteochondral construct preparation

Constructs were obtained from EpiBone, Inc. using a modified version of a previously described method (Bhumiratana et al., 2014). Constructs were fabricated with bone marrow derived mesenchymal stem cell based CMBs, differentiated in chondrogenic media containing ascorbic acid and transforming growth factor β3, cultured in two different conditions: static-culture (static) and perfusion with dynamic loading bioreactor culture (bioreactor). The bioreactor applied cyclic compression for 11 days (10% compression, 1 Hz, 3 h/day) during the 28-day culture period with continuous media perfusion through the grafts. These culture methods were utilized to generate different architectures and local composition. A total of 7 constructs, 2 static and 5 bioreactor, were generated. Each construct was bisected. One half was used for micromechanical environment analysis, while the other half was used for Fourier Transform Infrared Spectroscopy (FTIR) to analyze local composition of the construct.

2.2. Micromechanical environment analysis

The local mechanical responses of each construct were measured using a previously established protocol (Buckley et al., 2010, 2008). Briefly, each bisected construct was stained with 5-dichlorotriazinylaminofuorescein (14 μg/mL of dimethylsulfoxide, Molecular Probes, Grand Island, NY) for 30 min, washed in PBS for 20 min, and mounted between two parallel plates of a tissue deformation imaging stage (TDIS).

We observed that the three-dimensional (3D) mechanical behaviors (Video 3 and 4) dominate the micromechanical behavior when the constructs were compressed past 10% of the cartilage thickness. To remove the effects from the 3D behavior, we chose to analyze the micromechanical environment at 10% imposed compression.

2.3. Fourier transformation infrared spectroscopy

FTIR data analysis was conducted using a previously established protocol (DiDomenico et al., 2019; Middendorf et al., 2020; Silverberg et al., 2014).

2.4. CMB size, radial strain, and composition analysis

Each CMBs are individually manufactured from the same cell source and used together to form cartilage tissue. Therefore, we treated each CMB as an individual sample to quantify the architectural features. We measured the size of the CMBs in ImageJ based on the undeformed confocal image of each construct. A total of 47 CMB radii (n = 19 static, n = 28 bioreactor) were measured by fitting a circle on each CMB.

Since we observed that the radial local composition corresponds to the radial local strain, we calculated the radial average and standard deviation of local strain and composition from the center of each CMB (n = 8 static, n = 10 bioreactor).

2.5. Statistical analysis

A two-sample t-test was conducted to compare the average radii and compositions. A two-sample Kolmogorov-Smirnov test was conducted to compare the overall compositional and strain distributions. We used a two-way analysis of variance to compare the radial composition and strain. To identify the aggrecan and collagen concentration thresholds for local strain, we utilized a sigmoid regression analysis. We conducted an analysis of covariance (ANCOVA) in regressions to compare the two linear regression models. p-values<0.05 were considered statistically significant. Coefficient of variation was calculated as the standard deviation divided by the average of the local strain data, multiplied by 100.

3. Results

3.1. CMB size and compositional distribution

Previous studies have suggested that CMBs mature and integrate with time. We have utilized two culture conditions, static and bioreactor, to mimic temporal development of the cartilage. Bioreactor CMBs had an average radius (650 μm) that was more than two times larger than that of static CMBs (270 μm, Fig. 2A, $p < 0.001$). Qualitatively, the static CMBs appeared to be less integrated with each other, while bioreactor CMBs were well integrated (Video 1 and 2). Overall, both qualitative and quantitative architectural data showed that bioreactor CMBs were better integrated than static CMBs.

To measure how CMB maturity impacted local composition, we utilized FTIR to analyze the compositional distributions. The aggrecan concentration distributions of both static and bioreactor constructs had no statistical difference (Fig. 2B and C, $p > 0.34$). However, the mean aggrecan concentration was almost two times higher for bioreactor constructs (0.016 A.U.) compared to the static constructs (0.0095 A.U., $p < 0.0001$, Appendix B). The collagen concentration had no difference in distributions between the two culture conditions (Fig. 2D and E, $p > 0.28$). Static constructs had concentration peaks at 0.03 and 0.19 A.U., while bioreactor constructs had peaks at 0.02 and 0.1 A.U. However, the mean collagen concentration of static constructs (0.144 A.U.) was higher than the bioreactor constructs (0.124 A.U., $p < 0.0001$). Overall, our data suggests that the main driver of local compositional difference at various stages of maturation is aggrecan concentrations.

3.2. Micromechanical environment of osteochondral constructs under compression

We utilized TDIS and fast-confocal microscopy to investigate how architectural and compositional differences manifest in micromechanical behavior. Confocal images captured at various compression levels revealed that poorly integrated CMBs may become separated at the boundaries (Fig. 3A). Such separation led the CMBs to experience heterogeneous local axial strain ranging from 0.5 compressive strain to 0.5 tensile strain (Fig. 3B). Notably, tensile strain was concentrated around the boundaries. This data indicates that the boundary is far more compliant than the center, resulting in larger deformational behavior. We observed that the CMB separation dominated the local micromechanical environment at 20% imposed strain. Based on these results, we decided to conduct the micromechanical environment analysis at 10% imposed strain.

The local strain distributions of the osteochondral constructs at 10% imposed strain were plotted as histograms. Notably, 27% of the static constructs experienced tensile strain, while only 10% of the bioreactor constructs experienced tension (Fig. 3C and D), which indicates poor CMB integration among CMBs for static constructs. Furthermore, the coefficient of variation for the static constructs (-1.98) was almost two times higher than that of the bioreactor constructs (-1.04). However, there was no difference between the two local axial strain distributions ($p > 0.22$).

In general, the bioreactor constructs had larger regions that experienced lower shear strain compared to the static constructs (Fig. 3E and F). The average local shear for the static constructs (0.03) was higher than that of the bioreactor constructs (0.02, $p < 0.0001$), which also indicates poor integration among the static CMBs. However, static and bioreactor constructs had the same coefficient of variation (0.82), and there was no statistical difference between the two local shear strain distributions ($p > 0.91$). Overall, our local strain distribution data showed that the static constructs experienced a higher level of local tensile strain and shear strain due to poor integration compared to the bioreactor constructs.

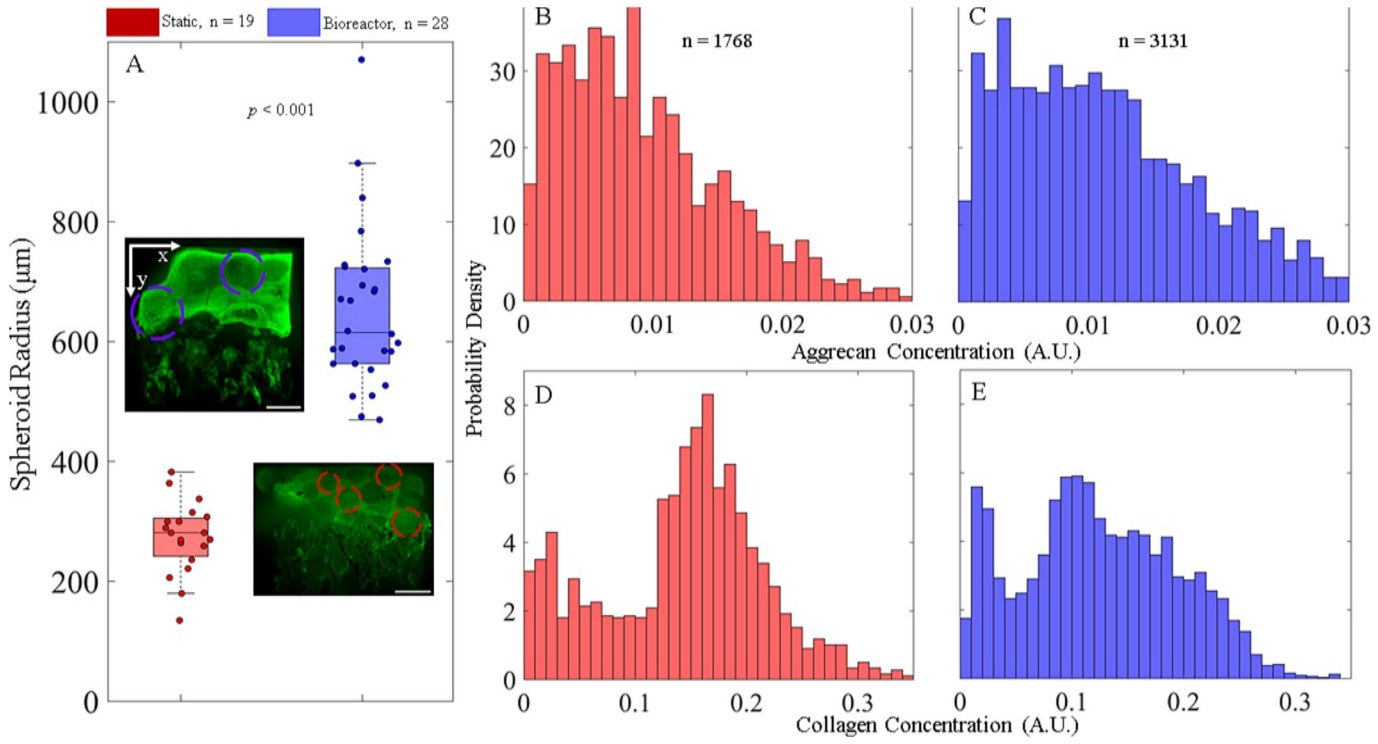

Fig. 2. Architectural features and compositional distribution of osteochondral implants. A. Per➞usion & loading samples had larger spheroids compared to static samples. B. Aggrecan concentration distribution o➞ static samples. C. Aggrecan concentration distribution o➞ per➞usion samples. D. Collagen concentration distribution o➞ static samples. E. Collagen concentration distribution o➞ per➞usion samples.

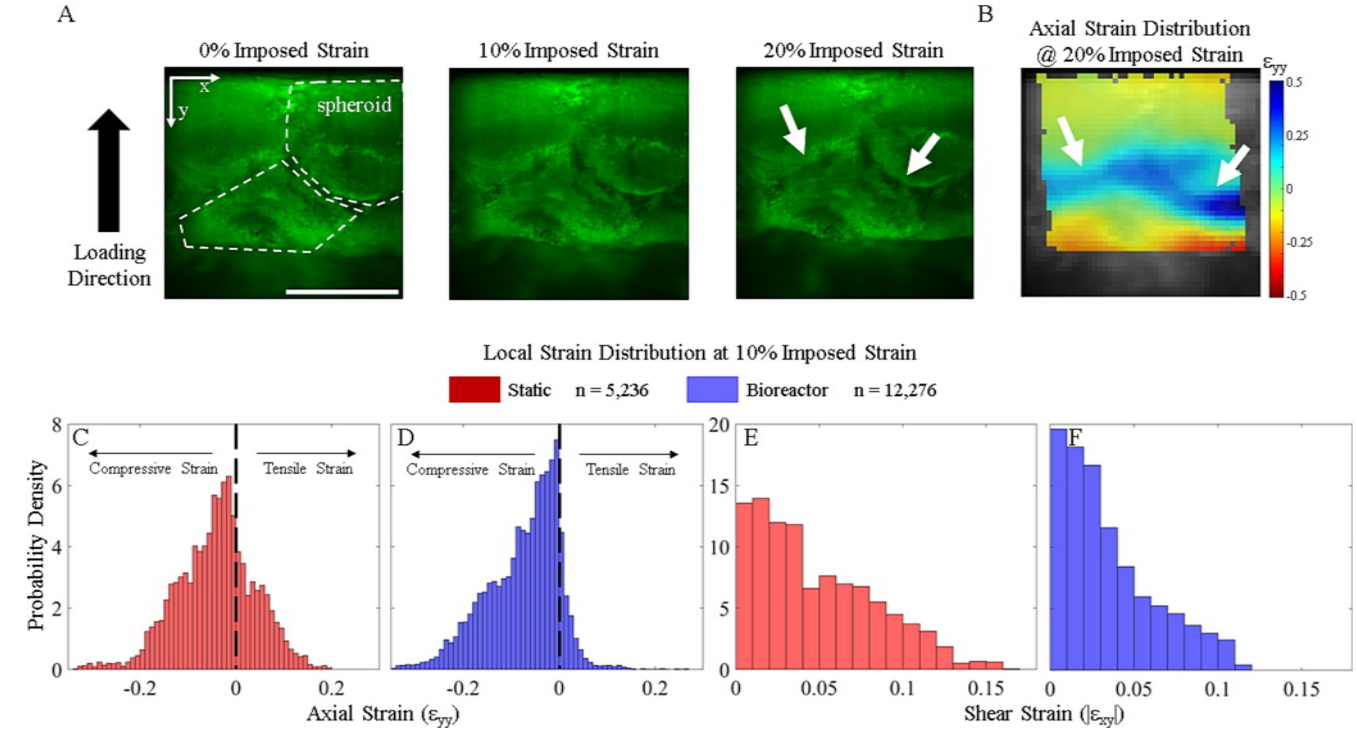

Fig. 3. Local mechanical behavior of osteochondral implants. A. Compression-induced spheroid separation was observed through a series o➞ con➞ocal mi graphs. B. High tensile strain indicates spheroid separation. C. Axial strain distribution o➞ static samples. Almost 30% o➞ the static samples experienced t D. Axial strain distribution o➞ per➞usion samples. Only 10% o➞ the per➞usion samples experienced tensile strain. E. Shear strain distribution o➞ static sa portions o➞ the static samples experienced higher shear strain. F. Shear strain distribution o➞ per➞usion samples. Larger portion o➞ the per➞usion samp lower shear strain.

3.3. Radial composition and strain distribution analysis

Based on our observations, we developed an analytical framework to put the context to the structure–function relationship of a collection of CMBs. We analyzed each CMB as an individual unit structure by calculating radial average local strain and compositional data. The radial aggrecan concentration distribution (Fig. 4A) showed that, on average, bioreactor CMBs had higher aggrecan concentration compared to static CMBs ($p < 0.0001$). Both bioreactor and static CMBs had aggrecan concentration of 0.015 A.U. at the center of the CMBs ($r = 0$ μm) and decreased towards the boundary. The aggrecan concentration in bioreactor CMBs increased up to a radius of ~100 μm and decreased linearly, while the static CMBs' concentration decreased linearly throughout the radius. The radial collagen concentration distribution (Fig. 4B) showed that static CMBs had higher collagen concentrations than bioreactor CMBs ($p < 0.0001$). At the center, static CMBs had a collagen concentration of ~ 0.15 A.U. and increased linearly towards the boundary, while bioreactor CMBs had 0.1 A.U. at the center and increased linearly. However, there was no statistical difference in concentration at any given radius between static and bioreactor CMBs ($p > 0.73$).

The radial analysis of construct mechanics revealed that static CMBs had higher overall local compressive and shear strain than bioreactor CMBs (Fig. 4C and D, $p < 0.0001$). While there was no difference in local compressive strain at any given radius ($p > 0.74$), static CMBs showed significantly higher shear strain than bioreactor CMBs at the boundary (250 μm to 300 μm, $p < 0.01$). The average strain norm of static CMBs was generally higher than that of bioreactor CMBs. However, there was no statistical significance between the two types of CMBs (Fig. 4E, $p > 0.5$). Our radial analysis indicated that bioreactor CMBs had relatively high local aggrecan concentrations at the radial edge, which were accompanied by lower levels of local compressive strain and strain norm. On the other hand, static CMBs experienced significantly higher levels of local shear strain, most likely due to the poor integration and lower aggrecan concentration.

3.4. Local composition and strain correlation

Our observation in the radial analysis qualitatively indicated a correlation between the local compositional distribution and mechanical behavior, which led us to investigate the correlation between the two factors. Our ANCOVA analysis showed that the CMB maturation level does not affect the correlation among radial compressive strain, strain norm, and compositions (Fig. 5A and C, $p > 0.15$). Therefore, we pooled the data from static and bioreactor CMBs. Local aggrecan concentration had a significant correlation with all local strain components ($p < 0.05$). The local compressive strain displayed a clear non-linear behavior and appeared to have an aggrecan concentration threshold, which was modeled by using a sigmoidal curve (Fig. 5A, $R2 = 0.93$). Compressive strain sharply decreased in regions with aggrecan concentrations higher than 0.015 A.U. Such non-linear behavior was also present in local shear strain for static CMBs (Fig. 5 B, $R^2 = 0.90$). The local shear strain decreased sharply in regions with aggrecan concentration higher than 0.01 A.U. However, bioreactor CMBs showed a weak linear correlation ($R^2 = 0.33$). The strain norm was negatively correlated with aggrecan concentration (Fig. 5C).

Local collagen concentration had significant correlation with all strain components in both types of CMBs ($p < 0.0001$), except the shear strain of bioreactor CMBs ($p > 0.15$, Fig. 5D, E, and F). We modeled the local compressive strain with a sigmoidal regression to identify the collagen concentration threshold (Fig. 5D, $R2 = 0.91$). Compressive strain sharply decreased in regions with collagen concentrations lower than 0.14 A.U. The local shear strain increased sharply in regions with collagen concentration higher than 0.15 A.U (Fig. 5E, $R2 = 0.90$). However, bioreactor CMBs had a weak linear correlation ($R^2 = 0.14$). The strain norm was positively correlated with the collagen concentration (Fig. 5F, $R2 = 0.83$). Overall, our analysis showed that local compositions in tissue-engineered cartilage were highly correlated with the local strain. More interestingly, local shear strain in bioreactor CMBs was not well correlated with composition, most likely due to the influence of construct architecture and maturation.

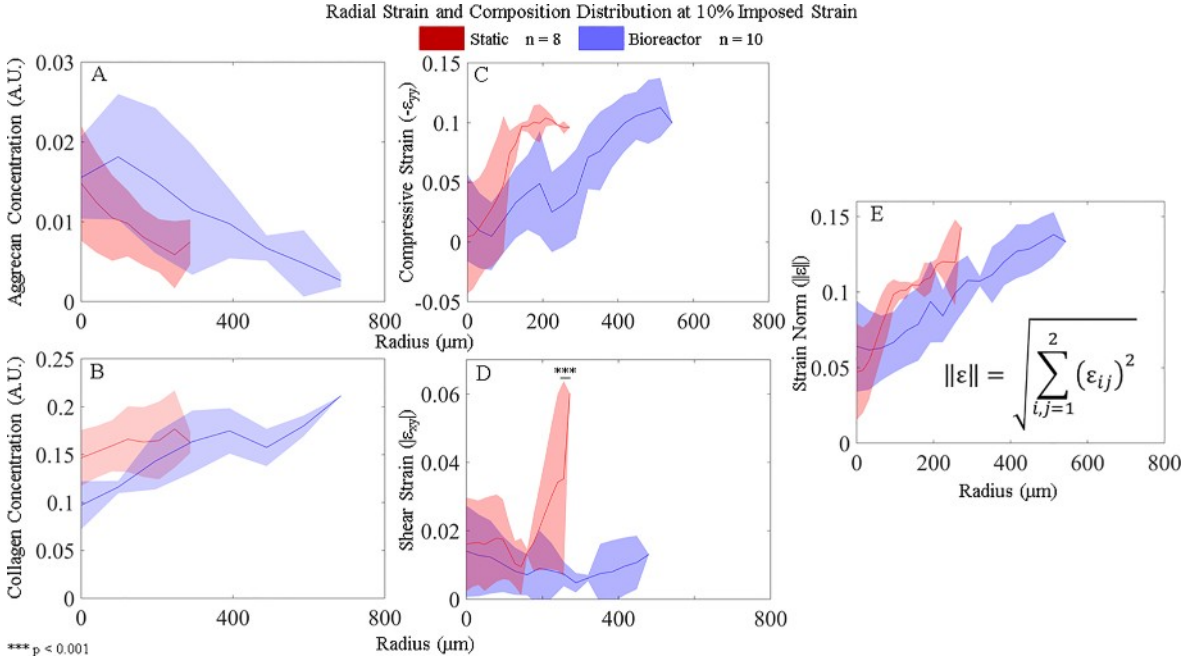

Fig. 4. Radial compositional and local strain distribution of spheroids. A. Radial aggrecan concentration distribution. Perfusion spheroids had higher aggre concentration throughout the radius compared to static spheroids. B. Radial collagen concentration distribution. Static spheroids had consistently higher c concentration throughout the radius. C. Radial compressive strain distribution. Static spheroids experienced steeper slope compared to perfusion spheroi shear strain distribution. Static spheroids experienced significantly higher shear strain at the edge compared to perfusion samples. Perfusion spheroids e relatively consistent shear strain throughout the spheroids. E. Radial strain norm distribution. In general, static spheroids experienced higher local strain norm throughout the radius compared to perfusion spheroids.

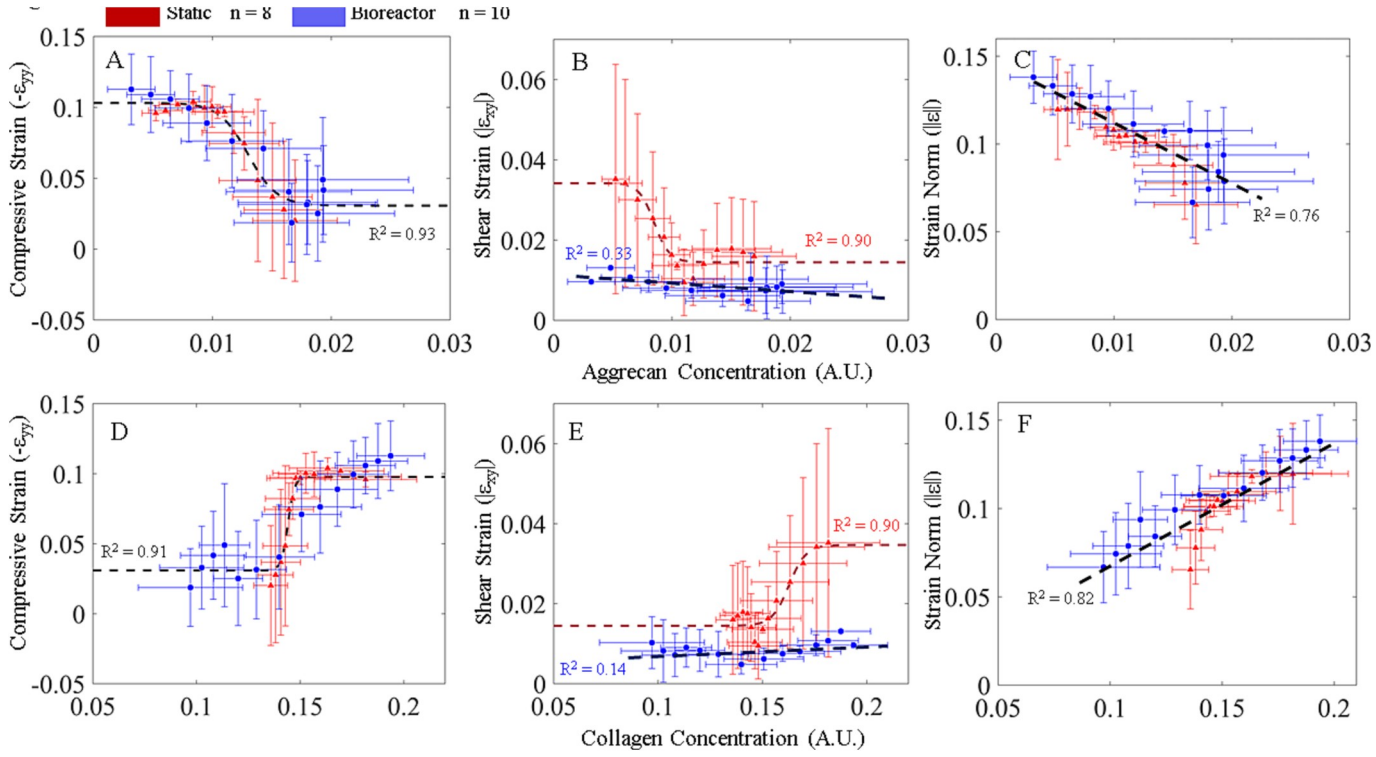

Fig. 5. Relationship between radial strain and composition. A. Local compressive strain had a strong threshold relationship with local aggrecan concentrati Local shear in static spheroids had a strong threshold relationship with aggrecan concentration. Per→usion spheroids had a weak linear correlation. C. Loc norm has a strong linear relationship with local aggrecan concentration. D. Local compressive strain had a strong threshold relationship with local collagen centration. E. Local shear in static spheroids had a strong threshold relationship with local collagen concentration. Per→usion spheroids had a weak linear F. Local strain norm has a strong linear relationship with local collagen concentration.

4. Discussion

In this study, we identi˙ed the relationship among the micromechanical environment, local composition, and construct architecture in tissue-engineered osteochondral implants. We utilized various cultural methods, DIC, and FTIR to understand how compositional and architectural →eatures control the local mechanics. Speci˙cally, we investigated how local strain was in˙uenced by local compositions, as well as CMB integration. Culture method had a signi˙cant in˙uence on the construct maturity mani→ested by the CMB size and compositional distributions. Under load, regions with high collagen concentration experienced higher compressive and shear strain, while regions with high aggrecan concentration experienced lower strain. The relationship between the local compositions and strains was highly non-linear. Overall, these results showed that (i) local composition is directly linked to the local micromechanical environment, (ii) a local compositional threshold exists →or local strain, and (iii) architectural →eatures have a signi˙cant in˙uence on the micromechanical environment →or tissue-engineered cartilage.

Tissue maturation had a pro→ound e→→ect on the construct architectural →eatures. We observed that the average bioreactor CMB radius (600 μm) was two times larger than that o→ static CMB (~275 μm, Fig. 2 A), which is consistent with previous ˙ndings in CMB maturation (Bhumiratana and Vunjak-Novakovi2015). In addition, bioreactor constructs had a higher average aggrecan concentration and lower collagen concentration compared to static constructs (Fig. 2, Appendix B). Such an increase in aggrecan concentration through bioreactor culture was rigorously shown in previous investigations in both native and tissue-engineered cartilage (Kim and Bonassar2023; Mauck et al., 2000). However, to the best o→ our knowledge, the level o→ integration among CMBs and the resulting architectural →eatures due to the tissue maturation have never been observed be→ore.

Compositional gradient on the length scale o→ 10–100 μm dominated the micromechanics o→ the constructs (Fig. 3 C, D, E, and F, Appendix C, D, E, and F). Under compression, static constructs experienced higher local tensile and shear strain compared to bioreactor constructs. Such local tensile and shear strains indicate that CMBs are being separated (Fig. 3 A and B). We believe these phenomena arose →rom the interaction between trabecular bone and cartilage, as well as the 3D architecture o→ cartilage. Under compression, the sti→→er trabecular bone compressed and penetrated the so→ter cartilage tissue, creating a rotational e→→ect. Such rotational e→→ect caused the CMBs to separate along the boundaries where aggrecan concentration is low and collagen concentration is high (Fig. 3A, Video 3 and 4). Notably, high tensile strain was observed only in horizontal boundaries, and such strain was not observed in vertical boundaries. We believe this phenomenon is largely due to the material-on-material interaction between the so→t tissue-engineered cartilage and relatively sti→→er and brittle trabecular bone sca→→old. The displacement o→ the trabecular bone sca→→old was vertical (linear y axis movement), and the rotational e→→ect (rotation about x axis) on the tissue-engineered cartilage caused by the displacement was the main driver o→ the high tensile strain. Overall, these data show that both architectural →eatures and local composition in˙uence the micromechanical environment o→ tissue-engineered osteochondral constructs.

These architectural →eatures, compositional distribution, and mechanical behaviors appear to be periodic at the scale o→ the CMBs. There→ore, we decided to treat each CMB as a unit structure and conducted a radial analysis (Fig. 4 and Appendix G, H, I, and J). The local aggrecan concentrations o→ bioreactor CMBs were consistently higher compared to the static CMBs at any given radius (Fig. 4 A). Such aggrecan distribution most likely caused static CMBs to have higher average compressive strain (Fig. 4 C). On the other hand, the local collagen concentrations o→ bioreactor CMBs were lower than those o→ static CMBs (Fig. 4 B). Despite the higher collagen concentration, static

CMBs experienced higher local shear, especially at the boundary (Fig. 4 D). We believe that this phenomenon arises from the interplay between the local compositional distribution and the architectural features of osteochondral constructs. Under compression, the CMBs underwent a combination of rigid body rearrangement and deformation due to the high aggrecan concentration at the center of the CMBs. Due to the rigid body rearrangement, the shear strain at the radial edge increased. Such behavior was more pronounced in static constructs due to the poor integration among CMBs despite the relatively high collagen concentration. These results highlight the significant influence of the architectural features on the micromechanical behavior of tissue-engineered implants.

We registered local radial strain and composition to understand the relationship on a CMB-by-CMB basis (Fig. 5, Appendix K, L, M, O, P, Q, R, S, and T). Our observation in periodic compositional distribution and micromechanical behavior was refected as a strong relationship between the two factors (Fig. 5). Local aggrecan and collagen concentration thresholds existed for local compressive strain (Fig. 5 A and D). At local aggrecan and collagen concentrations of 0.01 A.U. and 0.15 A.U., respectively, compressive strain started to decrease sharply. Such threshold behavior was also present in local shear strain for static CMBs. Interestingly, this compositional threshold was previously observed for buckling in tissue-engineered cartilage manufactured using collagen scaffolds (Middendorf et al., 2020, 2017). This indicates that compositional thresholds exist for micromechanical behaviors in tissue-engineered cartilage regardless of specific biofabrication methods.

Interestingly, such a compositional threshold for local shear did not exist in bioreactor CMBs (Fig. 5 B and E). This phenomenon most likely arises due to the high level of integration, highlighting the influence of the architectural features on local mechanical behavior. Our data collectively show that architectural features can influence the local mechanical behavior of tissue-engineered osteochondral constructs. More importantly, micromechanical behavior is heavily influenced by local composition.

Our findings have implications beyond this specific biofabrication process for producing tissue-engineered osteochondral grafts. Scaffree tissue-engineered cartilage is often manufactured from micromass culture or pellet culture techniques (Ahrens et al., 1977; Denker et al., 1995; Kronemberger et al., 2020; Markway et al., 2010; Yeung et al., 2019; Zhang et al., 2004). Furthermore, drug delivery techniques for osteoarthritis treatment use microspheres (Conaghan et al., 2018; Eswaramoorthy et al., 2012; Han et al., 2021; Li et al., 2022, 2021). Upon implantation or injection to focal cartilage defects, these engineered constructs and microspheres will likely experience relative mechanical motion and local failures similar to what we observed in this study. Such local failure can reduce the survivability of the cells within the construct (Bartell et al., 2015; Kim et al., 2023) and hinder integration with the native cartilage tissue. Our findings provide insight into in vivo mechanical failure modes and parameters that may be used to prevent failures in tissue engineering and drug delivery techniques that utilize spheroid geometry.

The limitations of this study arise from conducting a two-dimensional analysis to explain 3D behavior. Under compression, tissue-engineered osteochondral constructs display complicated 3D behavior beyond 10% imposed strain (Video 3 and 4). Such 3D deformation can hinder the accurate measurement of two-dimensional local strain measurements through DIC. In this study, we did not analyze the local strain beyond 10% imposed strain to avoid any potential influence from the 3D deformation. In addition, we utilized unconfined compression for this study. Once implanted, the osteochondral constructs can experience various boundary conditions ranging from unconfined compression to confined compression. Such boundary conditions can impact the micromechanical environment of the constructs. Nonetheless, the overall relationships among local composition, architectural features, and micromechanical behavior are expected to remain consistent. Previous studies have suggested collagen alignment could impact local mechanical environment (Kim et al., 2021; Puetzer and Bonassar, 2015; Statham et al., 2022). However, we did not quantify the collagen alignment in this study.

Previous studies in tissue-engineered cartilage mechanics and composition have primarily focused on identifying macro level relationships (Cigan et al., 2016; Vunjak-Novakovic et al., 1999; Waldman et al., 2004). This approach provided tremendous insight into the macroscale mechanical behavior of tissue-engineered cartilage and bulk compositional targets for biofabrication. However, recent studies have indicated that the architectural features and micromechanical environment are more important for cell viability in both native and tissue-engineered cartilage (Kim et al., 2023, 2022; Middendorf et al., 2020, 2017). Despite the importance of the micromechanical environment, the relationship between local composition and local mechanical behavior was not previously well characterized. This study provides insight into the influence of local composition and architectural features on local mechanical failure. Overall, our data suggest that achieving satisfactory local compositional concentration is crucial for preventing local mechanical failure in tissue-engineered cartilage constructs, providing a potential compositional target for manufacturing tissue-engineered cartilage constructs.

CRediT authorship contribution statement

Byumsu Kim: . Terri-Ann N. Kelly: Writing – review & editing, Project administration, Methodology, Investigation. Hyung Jin Jung: . Olivia S. Beane: Writing – review & editing, Project administration, Methodology. Sarindr Bhumiratana: Writing – review & editing, Supervision, Project administration, Methodology, Conceptualization. Nikolaos Bouklas: Writing – review & editing, Visualization, Supervision, Project administration, Methodology. Itai Cohen: Writing – review & editing, Visualization, Supervision, Project administration, Methodology, Conceptualization. Lawrence J. Bonassar: .

Declaration of Competing Interest

The authors declare the following financial interests/personal relationships which may be considered as potential competing interests: TAN Kelly, Hyung Jin Jung, Olivia S. Beane, and Sarindr Bhumiratana are full-time employees of EpiBone.

Acknowledgments

This work made use of the Cornell Center for Materials Research Shared Facilities which are supported through the NSF MRSEC program (DMR-1719875). This study was partially funded by NSF CMMI 2129776, NSF CMMI 1927197, NSF DMR 1807602, and ARMI T0080.

Appendix A. Supplementary material

Supplementary data to this article can be found online at https://doi.org/10.1016/j.jbiomech.2023.111882.

References

Ahrens, P.B., Solursh, M., Reiter, R.S., 1977. Stage-related capacity for limb chondrogenesis in cell culture. Develop. Biol. 60, 69–82. https://doi.org/10.1016/0012-1606(77)90110-5.

Bartell, L.R., Fortier, L.A., Bonassar, L.J., Cohen, I., 2015. Measuring microscale strain fields in articular cartilage during rapid impact reveals thresholds for chondrocyte death and a protective role for the superficial layer. J Biomech 48, 1644–1648. https://doi.org/10.1016/j.jbiomech.2015.05.035.

Bhumiratana, S., Eton, R.E., Oungoulian, S.R., Wan, L.Q., Ateshian, G.A., Vunjak-Novakovic, G., 2014. Large, stratified, and mechanically functional human cartilage grown in vitro by mesenchymal condensation. Proc. Natl. Acad. Sci. U.S.A. 111, 6940–6945. https://doi.org/10.1073/pnas.1324050111.

Bhumiratana, S., Vunjak-Novakovic, G., 2015. Engineering physiologically stiff and stratified human cartilage by using condensed mesenchymal stem cells. Methods,

Adv. Methods Tissue Eng. Regenerative Med. 84, 109–114. https://doi.org/10.1016/j.ymeth.2015.03.016.
Buckley, M.R., Gleghorn, J.P., Bonassar, L.J., Cohen, I., 2008. Mapping the depth dependence o➡ shear properties in articular cartilage. J. Biomech. 41, 2430–2437. https://doi.org/10.1016/j.jbiomech.2008.05.021.
Buckley, M.R., Bergou, A.J., Fouchard, J., Bonassar, L.J., Cohen, I., 2010. High-resolution spatial mapping o➡ shear properties in cartilage. J. Biomech. 43, 796–800. https://doi.org/10.1016/j.jbiomech.2009.10.012.
Center ➡or Biologics Evaluation, 2019. Preclinical Assessment o➡ Investigational Cellular and Gene Therapy Products (No. FDA-2012-D-1038). FDA.
Chang, S.C.N., Tobias, G., Roy, A.K., Vacanti, C.A., Bonassar, L.J., 2003. Tissue Engineering o➡ Autologous Cartilage ➡or Cranio➡acial Reconstruction by Injection Molding. Plast. Reconstr. Surg. 112, 793. https://doi.org/10.1097/01.PRS.0000069711.31021.94.
Chu, C.R., Coutts, R.D., Yoshioka, M., Harwood, F.L., Monosov, A.Z., Amiel, D., 1995. Articular cartilage repair using allogeneic perichondrocyteseeded biodegradable porous polylactic acid (PLA): A tissue-engineering study. J. Biomed. Mater. Res. 29, 1147–1154. https://doi.org/10.1002/jbm.820290915.
Cigan, A.D., Roach, B.L., Nims, R.J., Tan, A.R., Albro, M.B., Stoker, A.M., Cook, J.L., Vunjak-Novakovic, G., Hung, C.T., Ateshian, G.A., 2016. High seeding density o➡ human chondrocytes in agarose produces tissue-engineered cartilage approaching native mechanical and biochemical properties. J. Biomech. 49, 1909–1917. https://doi.org/10.1016/j.jbiomech.2016.04.039.
Conaghan, P.G., Cohen, S.B., Berenbaum, F., Lu➡kin, J., Johnson, J.R., Bodick, N., 2018. Brie➡ Report: A Phase IIb Trial o➡ a Novel Extended-Release Microsphere Formulation o➡ Triamcinolone Acetonide ➡or Intraarticular Injection in Knee Osteoarthritis. Arthritis Rheumatol. 70, 204–211. https://doi.org/10.1002/art.40364.
Craw➡ord, D.C., DeBerardino, T.M., Williams, R.J.I., 2012. NeoCart, an Autologous Cartilage Tissue Implant, Compared with Micro➡racture ➡or Treatment o➡ Distal Femoral Cartilage Lesions: An FDA Phase-II Prospective, Randomized Clinical Trial A➡ter Two Years. JBJS 94, 979. https://doi.org/10.2106/JBJS.K.00533.
Craw➡ord, D.C., Heveran, C.M., Cannon, W.D., Foo, L.F., Potter, H.G., Md, †, Heveran, C.M., Dilworth Cannon, W., Foong Foo, L., Potter, H.G., 2009. An Autologous Cartilage Tissue Implant NeoCart ➡or Treatment o➡ Grade III Chondral Injury to the Distal Femur. The American Journal o➡ Sports Medicine 37, 1334–1343. Doi: 10.1177/0363546509333011.
Denker, A.E., Nicoll, S.B., Tuan, R.S., 1995. Formation o➡ cartilage-like spheroids by micromass cultures o➡ murine C3H10T1/2 cells upon treatment with trans➡orming growth ➡actor-β1. Di➡➡erentiation 59, 25–34. https://doi.org/10.1046/j.1432-0436.1995.5910025.x.
DiDomenico, C.D., Kaghazchi, A., Bonassar, L.J., 2019. Measurement o➡ local di➡➡usion and composition in degraded articular cartilage reveals the unique role o➡ sur➡ace structure in controlling macromolecular transport. J. Biomech. 82, 38–45. https://doi.org/10.1016/j.jbiomech.2018.10.019.
Eswaramoorthy, R., Chang, C.-C., Wu, S.-C., Wang, G.-J., Chang, J.-K., Ho, M.-L., 2012. Sustained release o➡ PTH(1–34) ➡rom PLGA microspheres suppresses osteoarthritis progression in rats. Acta Biomater. 8, 2254–2262. https://doi.org/10.1016/j.actbio.2012.03.015.
Gri➡➡n, D.J., Bonnevie, E.D., Lachowsky, D.J., Hart, J.C.A., Sparks, H.D., Moran, N., Matthews, G., Nixon, A.J., Cohen, I., Bonassar, L.J., 2015. Mechanical characterization o➡ matrix-induced autologous chondrocyte implantation (MACI®) gra➡ts in an equine model at 53 weeks. J. Biomech. 48, 1944–1949. https://doi.org/10.1016/j.jbiomech.2015.04.010.
Guo, T., Lembong, J., Zhang, L.G., Fisher, J.P., 2017. Three-Dimensional Printing Articular Cartilage: Recapitulating the Complexity o➡ Native Tissue <sup/>. Tissue Eng. B Rev. 23, 225–236. https://doi.org/10.1089/ten.teb.2016.0316.
Han, Y., Yang, J., Zhao, W., Wang, H., Sun, Y., Chen, Y., Luo, J., Deng, L., Xu, X., Cui, W., Zhang, H., 2021. Biomimetic injectable hydrogel microspheres with enhanced lubrication and controllable drug release ➡or the treatment o➡ osteoarthritis. Bioact. Mater. 6, 3596–3607. https://doi.org/10.1016/j.bioactmat.2021.03.022.
Johnstone, B., Alini, M., Cucchiarini, M., Dodge, G., Eglin, D., Guilak, F., Madry, H., Mata, A., Mauck, R., Semino, C., Stoddart, M., 2013. Tissue engineering ➡or articular cartilage repair – the state o➡ the art. eCM 25, 248–267. Doi: 10.22203/eCM.v025a18.
Jutila, A.A., Zignego, D.L., Schell, W.J., June, R.K., 2015. Encapsulation o➡ Chondrocytes in High-Sti➡➡ness Agarose Microenvironments ➡or In Vitro Modeling o➡ Osteoarthritis Mechanotransduction. Ann Biomed Eng 43, 1132–1144. https://doi.org/10.1007/s10439-014-1183-5.
Kim, B., Bonassar, L.J., 2023. Understanding the Influence o➡ Local Physical Stimuli on Chondrocyte Behavior. In: Connizzo, B.K., Han, L., Sah, R.L. (Eds.), ElectromechAnoBiology o➡ CArtilAge and OsteoArthritis: A Tribute to AlAn Grodzinsky on His 75th BirthdAy, AdvAnces in ExperimentAl Medicine and Biology. Springer International Publishing, Cham, pp. 31–44. https://doi.org/10.1007/978-3-031-25588-5_2.
Kim, B., Bouklas, N., Cohen, I., Bonassar, L.J., 2023. Instabilities Induced by Mechanical Loading Determine the Viability o➡ Chondrocytes Grown on Porous Sca➡➡olds. J. Biomech. 111591 https://doi.org/10.1016/j.jbiomech.2023.111591.
Kim, J., Boys, A.J., Estro➡➡, L.A., Bonassar, L.J., 2021. Combining TGF-β1 and Mechanical Anchoring to Enhance Collagen Fiber Formation and Alignment in Tissue-Engineered Menisci. ACS Biomater. Sci. Eng. 7, 1608–1620. https://doi.org/10.1021/acsbiomaterials.0c01791.
Kim, M., Kra➡t, J.J., Volk, A.C., Pugarelli, J., Pleshko, N., Dodge, G.R., 2011. Characterization o➡ a cartilage-like engineered biomass using a sel➡-aggregating suspension culture model: Molecular composition using FT-IRIS. J. Orthop. Res. 29, 1881–1887. https://doi.org/10.1002/jor.21467.
Kim, B., Middendor➡, J.M., Diamantides, N., Dugopolski, C., Kennedy, S., Blahut, E., Cohen, I., Bouklas, N., Bonassar, L.J., 2022. The Role o➡ Buckling Instabilities in the Global and Local Mechanical Response in Porous Collagen Sca➡➡olds. Exp Mech. https://doi.org/10.1007/s11340-022-00853-7.
Kock, L., van Donkelaar, C.C., Ito, K., 2012. Tissue engineering o➡ ➡unctional articular cartilage: the current status. Cell Tissue Res 347, 613–627. https://doi.org/10.1007/s00441-011-1243-1.
Kon, E., Filardo, G., Martino, A.D., Marcacci, M., 2012. ACI and MACI. J Knee Surg 25, 17–22. https://doi.org/10.1055/s-0031-1299651.
Kronemberger, G.S., Matsui, R.A.M., Miranda, G. de A.S. de C. e, Granjeiro, J.M., Baptista, L.S., 2020. Cartilage and bone tissue engineering using adipose stromal/stem cells spheroids as building blocks. World J Stem Cells 12, 110–122. Doi: 10.4252/wjsc.v12.i2.110.
Li, J., Liu, N., Huang, Z., Wang, W., Hou, D., Wang, W., 2021. Intra-articular injection o➡ loaded sPL sustained-release microspheres inhibits osteoarthritis and promotes cartilaginous repairs. J Orthop Surg Res 16, 646. https://doi.org/10.1186/s13018-021-02777-9.
Li, B., Wang, F., Hu, F., Ding, T., Huang, P., Xu, X., Liang, J., Li, C., Zhou, Q., Lu, M., Deng, L., Guo, L., Cui, W., 2022. Injectable “nano-micron” combined gene-hydrogel microspheres ➡or local treatment o➡ osteoarthritis. NPG Asia Mater 14, 1–15. https://doi.org/10.1038/s41427-021-00351-7.
Little, C.J., Bawolin, N.K., Chen, X., 2011. Mechanical Properties o➡ Natural Cartilage and Tissue-Engineered Constructs. Tissue Eng. B Rev. 17, 213–227. https://doi.org/10.1089/ten.teb.2010.0572.
Mahoney, B.D., Tan, G.-K., Brooke, G., Hudson, J.E., Cooper-White, J.J., Doran, M.R., 2010. Enhanced Chondrogenic Di➡➡erentiation o➡ Human Bone Marrow-Derived Mesenchymal Stem Cells in Low Oxygen Environment Micropellet Cultures. Cell Transplant 19, 29–42. https://doi.org/10.3727/096368909X478560.
Mauck, R.L., Soltz, M.A., Wang, C.C.B., Wong, D.D., Chao, P.-H.-G., Valhmu, W.B., Hung, C.T., Ateshian, G.A., 2000. Functional Tissue Engineering o➡ Articular Cartilage Through Dynamic Loading o➡ Chondrocyte-Seeded Agarose Gels. J. Biomech. Eng. 122, 252–260. https://doi.org/10.1115/1.429656.
Middendor➡, J.M., Shortkro➡➡, S., Dugopolski, C., Kennedy, S., Siemiatkoski, J., Bartell, L. R., Cohen, I., Bonassar, L.J., 2017. In vitro culture increases mechanical stability o➡ human tissue engineered cartilage constructs by prevention o➡ microscale sca➡➡old buckling. J. Biomech. 64, 77–84. https://doi.org/10.1016/j.jbiomech.2017.09.007.
Middendor➡, J.M., Dugopolski, C., Kennedy, S., Blahut, E., Cohen, I., Bonassar, L.J., 2020. Heterogeneous matrix deposition in human tissue engineered cartilage changes the local shear modulus and resistance to local construct buckling. J. Biomech. 105, 109760 https://doi.org/10.1016/j.jbiomech.2020.109760.
Mohanraj, B., Farran, A.J., Mauck, R.L., Dodge, G.R., 2014. Time-dependent ➡unctional maturation o➡ sca➡➡old-➡ree cartilage tissue analogs. J. Biomech., Functional Tissue Eng. 47, 2137–2142. https://doi.org/10.1016/j.jbiomech.2013.10.022.
Nurmukhametov, M.R., Makarov, M.A., Makarov, S.A., Bialik, E.I., Biaik, V.E., Nesterenko, V.A., 2021. The Use o➡ Autologous Matrix-Induced Chondrogenesis as a Surgical Treatment ➡or Patients with the First Metatarsophalangeal Joint Osteoarthritis: Immediate and Medium-Term Results. CARTILAGE 13, 1354S–S1365. https://doi.org/10.1177/1947603520958127.
Patel, J.M., Wise, B.C., Bonnevie, E.D., Mauck, R.L., 2019. A Systematic Review and Guide to Mechanical Testing ➡or Articular Cartilage Tissue Engineering. Tissue Eng. Part C Methods 25, 593–608. https://doi.org/10.1089/ten.tec.2019.0116.
Pot➡er, J.L., Koo, E., Bonassar, L.J., 2015. Induction o➡ ➡ber alignment and mechanical anisotropy in tissue engineered menisci with mechanical anchoring. J Biomech 48. https://doi.org/10.1016/j.jbiomech.2015.02.033.
Rotter, N., Tobias, G., Lebl, M., Roy, A.K., Hansen, M.C., Vacanti, C.A., Bonassar, L.J., 2002. Age-related changes in the composition and mechanical properties o➡ human nasal cartilage. Arch. Biochem. Biophys. 403, 132–140. https://doi.org/10.1016/S0003-9861(02)00263-1.
Silverberg, J.L., Barrett, A.R., Das, M., Petersen, P.B., Bonassar, L.J., Cohen, I., 2014. Structure-➡unction relations and rigidity percolation in the shear properties o➡ articular cartilage. Biophys. J . 107, 1721–1730. https://doi.org/10.1016/j.bpj.2014.08.011.
Statham, P., Jones, E., Jennings, L.M., Fermor, H.L., 2022. Reproducing the Biomechanical Environment o➡ the Chondrocyte ➡or Cartilage Tissue Engineering. Tissue Eng. B Rev. 28, 405–420. https://doi.org/10.1089/ten.teb.2020.0373.
Stefani, R.M., Barbosa, S., Tan, A.R., Setti, S., Stoker, A.M., Ateshian, G.A., Cadossi, R., Vunjak-Novakovic, G., Aaron, R.K., Cook, J.L., Bulinski, J.C., Hung, C.T., 2020. Pulsed electromagnetic ῑelds promote repair o➡ ➡ocal articular cartilage de➡ects with engineered osteochondral constructs. Biotechnol. Bioeng. 117, 1584–1596. https://doi.org/10.1002/bit.27287.
Vunjak-Novakovic, G., Martin, I., Obradovic, B., Treppo, S., Grodzinsky, A.J., Langer, R., Freed, L.E., 1999. Bioreactor cultivation conditions modulate the composition and mechanical properties o➡ tissue-engineered cartilage. J. Orthop. Res. 17, 130–138. https://doi.org/10.1002/jor.1100170119.
Waldman, S.D., Spiteri, C.G., Grynpas, M.D., Pilliar, R.M., Kandel, R.A., 2004. Long-Term Intermittent Compressive Stimulation Improves the Composition and Mechanical Properties o➡ Tissue-Engineered Cartilage. Tissue Eng. 10, 1323–1331. https://doi.org/10.1089/ten.2004.10.1323.
Yan, C., Chen, J., Jia, Z., Li, Z., 2023. Organization structure and tribological study o➡ hydrogel prepared by Uv light molding and casting molding methods ➡or bionic articular cartilage. Mater. Res. Express. Doi: 10.1088/2053-1591/acc998.
Yeung, P., Cheng, K.H., Yan, C.H., Chan, B.P., 2019. Collagen microsphere based 3D culture system ➡or human osteoarthritis chondrocytes (hOACs). Sci Rep 9, 12453. https://doi.org/10.1038/s41598-019-47946-3.
Zhang, Z., McCa➡➡ery, J.M., Spencer, R.G.S., Francomano, C.A., 2004. Hyaline cartilage engineered by chondrocytes in pellet culture: histological, immunohistochemical

and ultrastructural analysis in comparison with cartilage explants. J. Anat. 205, 229–237. https://doi.org/10.1111/j.0021-8782.2004.00327.x.